

Self-electroforming and high-performance complementary memristor based on ferroelectric tunnel junctions

Cite as: Appl. Phys. Lett. **109**, 053506 (2016); <https://doi.org/10.1063/1.4960523>

Submitted: 26 April 2016 . Accepted: 22 July 2016 . Published Online: 04 August 2016

Z. B. Yan, H. M. Yau, Z. W. Li, X. S. Gao, J. Y. Dai, and J.-M. Liu 



View Online



Export Citation



CrossMark

ARTICLES YOU MAY BE INTERESTED IN

[Ferroelectric memristor based on Pt/BiFeO₃/Nb-doped SrTiO₃ heterostructure](#)

Applied Physics Letters **102**, 102901 (2013); <https://doi.org/10.1063/1.4795145>

[Tunnel electroresistance in BiFeO₃ junctions: size does matter](#)

Applied Physics Letters **109**, 232902 (2016); <https://doi.org/10.1063/1.4971311>

[Effect of a semiconductor electrode on the tunneling electroresistance in ferroelectric tunneling junction](#)

Applied Physics Letters **109**, 163501 (2016); <https://doi.org/10.1063/1.4965708>

Lock-in Amplifiers
Find out more today



 Zurich Instruments

Self-electroforming and high-performance complementary memristor based on ferroelectric tunnel junctions

Z. B. Yan,^{1,2,a)} H. M. Yau,² Z. W. Li,³ X. S. Gao,³ J. Y. Dai,^{2,a)} and J.-M. Liu^{1,3,a)}

¹Laboratory of Solid State Microstructures and Innovation Center of Advanced Microstructures, Nanjing University, Nanjing 210093, China

²Department of Applied Physics, Hong Kong Polytechnic University, Kowloon, Hong Kong, China

³Institute for Advanced Materials and Laboratory of Quantum Engineering and Quantum Materials, South China Normal University, Guangzhou 510006, China

(Received 26 April 2016; accepted 22 July 2016; published online 4 August 2016)

Complementary resistive switching (CRS) has potential applications in ultra-high density three-dimensional crossbar arrays for resistive random access memories and Logic-in-Memories. For real applications, the good stability and electroforming-free character have become essential prerequisites. In this work, we investigate the resistance switching behaviors of a CRS device based on two anti-serial Au/BaTiO₃/Nb:SrTiO₃ ferroelectric tunnel junctions (FTJs). This FTJ-based CRS device shows a stable butterfly-like resistance-voltage hysteresis, as well as self-electroforming, multi-switching, and good performance complementary switching behaviors. The present work presents a convincing demonstration of the complementary multi-switching states modulated by remnant ferroelectric polarization, making the FTJ structure good potentials for high-performance CRS memristors. *Published by AIP Publishing.* [<http://dx.doi.org/10.1063/1.4960523>]

Recently, complementary resistive switching (CRS) has been greatly concerned not only for solving the sneak-path problem in the ultra-dense passive crossbar resistive memory (RRAM) arrays^{1,2} but also for providing the inherent System-on-Memory and Logic-in-Memory (LIM) capabilities.^{3–5} A CRS structure is composed of two anti-serial bipolar resistive memory elements sharing a common electrode.⁶ The memory elements used in CRS in earlier reports are usually the filament-type memristors including the valence change memories (VCMs) and electrochemical metallization cells (ECMs), which offer excellent endurance, retention, and scaling properties.^{7–11} However, such memory elements usually need an electroforming process prior to operation and often generate large perturbations on the critical read/write voltage windows.¹² For the CRS with crossbar arrays, the voltage drops along the lines hinder application of the same electroforming voltage to each element, making it difficult to electroform uniformly all the memory elements.¹² Therefore, any approach to develop electroforming-free or self-electroforming memory elements is highly preferred for CRS devices.¹³ Besides, the large variation of critical read/write voltage windows in each memory element has become a major obstacle for applications.¹⁴

Ferroelectric tunnel junctions (FTJs) may be excellent candidates for avoiding the above addressed issues in high performance CRS devices.¹⁵ A FTJ is composed of an ultrathin (usually thinner than 10 nm) ferroelectric film sandwiched by two electrodes.¹⁶ As an external voltage is applied to the two electrodes, a leakage current flows through the FTJ barrier via various mechanisms such as direct tunneling, Fowler–Nordheim tunneling, and/or thermionic emission.¹⁷ Upon a positive or negative voltage pulse, the ferroelectric switching strongly modulates the ferroelectric/electrode

junction barrier, generating an electro-resistance effect with a high OFF/ON resistance ratio.^{17–19} Owing to the inherent property, the ferroelectric film owns stable coercive field and polarization. The usage of FTJs in a CRS structure will ensure the high stability of critical read/write voltage windows, excellent endurance, and good retention. Furthermore, a CRS device composed of FTJs is self-electroforming and may offer multi-switching functionality, as to be demonstrated in this work.

We fabricated ultrathin ferroelectric BaTiO₃ (BTO) films on 0.7 wt. % Nb-doped SrTiO₃ (100) (NSTO) single crystal substrates by the laser-molecular beam epitaxy (Laser-MBE). The laser fluence, laser repetition rate, base pressure, oxygen ambient pressure, and growth temperature are 200 mJ, 1 Hz, 2.0×10^{-5} Pa, 10 Pa, and 700 °C, respectively. After the deposition, the samples were *in-situ* annealed at 700 °C under a high oxygen pressure of 0.1 atm (10 kPa) for 1 h. The Au electrodes with 200 μm in diameter were deposited by ion sputtering with a shadow mask. The resistance switching performances were measured by the two-probe method using a Keithley 2636A source-meter with home-made software.

Fig. 1(a) shows a cross-sectional high-resolution transmission electron microscopy (TEM) image of an ultrathin BTO film on a NSTO substrate, where a uniform BTO layer of ~3.0 nm in thickness can be clearly seen. The high-resolution TEM image of the BTO film, as shown in Fig. 1(b), reveals the excellent epitaxial growth of BTO on NSTO.

Because the separation between two nearest-neighbor top Au electrode dots is much bigger than the BTO film thickness, the top-top measurement configuration, as schematically shown in Fig. 1(c), allows us to study the CRS performance on the present Au/BTO/NSTO/BTO/Au structure. Fig. 1(d) shows the current-voltage (*I*-*V*) hysteresis measured at room temperature with the top-top electrode configuration. The *I*-*V* hysteresis loop is clockwise rotating in both the positive and negative voltage regions and does not

^{a)} Authors to whom correspondence should be addressed. Electronic addresses: zbyan@nju.edu.cn; jiyuan.dai@polyu.edu.hk; and liujm@nju.edu.cn

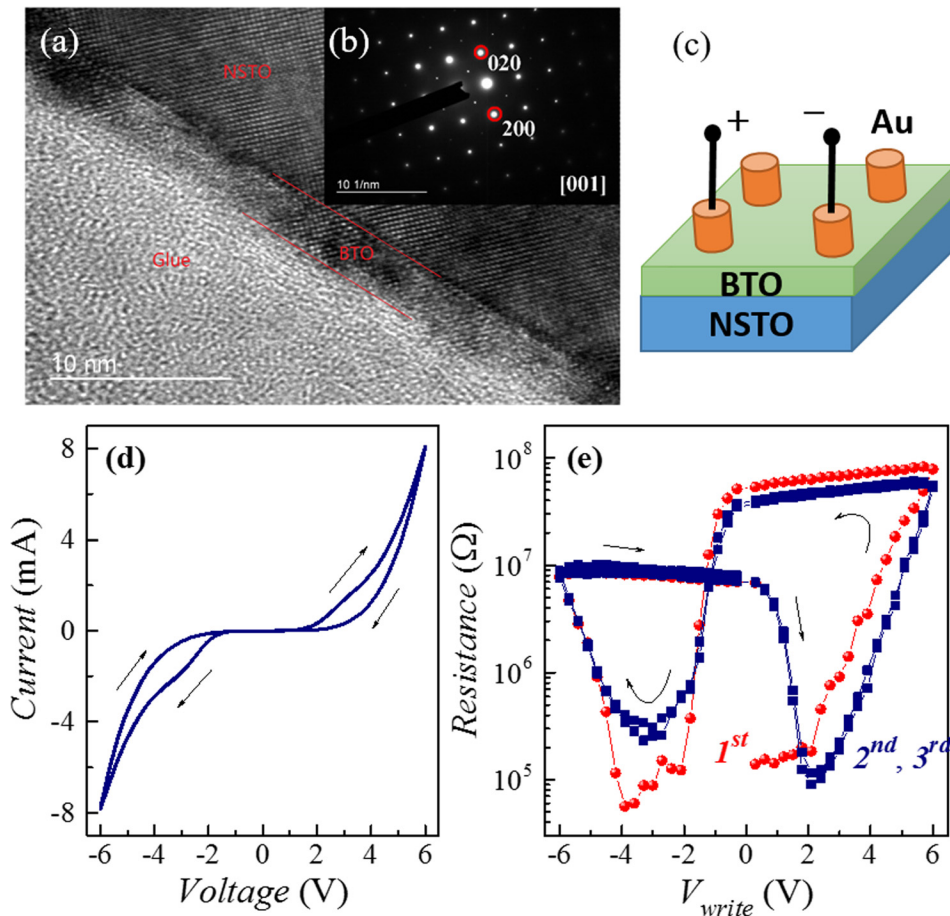


FIG. 1. Structure of the BTO/NSTO heterostructure: (a) High-resolution TEM image of the BTO/NSTO of the selected region; (b) The electron diffraction pattern of the BTO/NSTO heterostructure. (c) Schematic of the measurement configuration. (d) Current-voltage behavior of Au/BTO/NSTO junctions, measured with top-top electrode configuration. (e) Butterfly-like R - V_{write} hysteresis loops under the three continuous rounds of V_{write} -sweep, measured by 0.5 V after the operation of each V_{write} pulse (pulse-on: 10 ms, pulse-off 1.0 s).

crossover at $V=0$. A specific but highly favored character is that the two loop windows appear in gaps $[-6.0\text{ V}, -1.0\text{ V}]$ and $[1.0\text{ V}, 6.0\text{ V}]$, respectively, leaving zero current in gap $[-1.0\text{ V}, 1.0\text{ V}]$, demonstrating a typical complementary memory behavior which is well described in the literature.¹

To demonstrate how the CRS works as driven by the writing voltage pulse (V_{write}), we measured the V_{write} -dependent resistance (R) hysteresis, where the resistances were read by a low voltage of 0.5 V after each V_{write} pulse (with 10 ms pulse-on and 1.0 s pulse-off time), respectively. Fig. 1(e) presents three R - V_{write} hysteresis loops measured in sequence on a fresh device with $V_{write} \in [-6.0\text{ V}, 6.0\text{ V}]$. The initial state is stayed at a low resistance (LR) state with a resistance of $\sim 0.1\text{ M}\Omega$. During the first sweep from 0 to 2.1 V, the device stays at the initial state. Subsequently, the device resistance increases dramatically and reaches a high resistance (HR) state of resistance $\sim 70\text{ M}\Omega$ at 6 V. Interestingly, this HR state remains nearly invariable in the subsequent sweep from 6.0 V to -0.3 V , generating a HR platform. Then, the resistance begins to decrease, goes through a minimum point of $\sim 0.58\text{ M}\Omega$ at -3.3 V , comes to the left-edge of second HR platform ($\sim 1.2\text{ M}\Omega$) at -6.0 V , and finally remains at this HR platform during the back sweep from -6.0 V to 0. In the second cycle, the CRS device starts from the second HR platform, goes through another minimum point at $\sim 2.1\text{ V}$ with a resistance close to the initial state of the first cycle, and then follows the track of the first cycle R - V_{write} hysteresis loop. The whole hysteresis displays a butterfly-like pattern. At the voltage of the minimum point in R - V_{write} hysteresis loop, the I - V curve also shows small humps. In the third cycle (and in

fact the subsequent many cycles), the R - V_{write} hysteresis almost completely follows that of the second cycle, demonstrating the good reproducibility of the butterfly-like R - V_{write} hysteresis upon the cycling. This evolution indicates that there is no need for electroforming on each memory element in the CRS device. The first V_{write} -sweep cycling automatically completes the uniform electroforming process.

Naturally, this butterfly-like hysteresis will be degraded into a parallelogram-like hysteresis if V_{write} covers only one critical voltage. Fig. 2(a) shows the butterfly-like and parallelogram-like I - V_{write} loops under the $[-6.0\text{ V}, 6.0\text{ V}]$ and $[-3.3\text{ V}, 6.0\text{ V}]$ sweeps, respectively. For the latter sweep, the data from 6.0 V to -3.3 V are coincident with the data from the $[-6.0\text{ V}, 6.0\text{ V}]$ sweep. However, upon the backward sweep from -3.3 V , a LR state remains unchanged until V_{write} is higher than the positive critical voltage ($\sim 2.0\text{ V}$), generating a LR platform in the $[-3.3\text{ V}, 2.0\text{ V}]$ range. This result suggests that a CRS device can be switched between different resistance states upon different end V_{write} , showing a multi-switching functionality.

To study the multi-switching effect, we used the pulses of 6.0 V, -6.0 V , and 2.4 V in sequence to obtain the assigned **A**, **B**, and **C** states, respectively. Fig. 2(b) demonstrates the good endurance and reliability of multi-switching between these states over more than 3000 cycles. Besides, the CRS device can be switched between any two different states using simple pulse assignment. For example, Fig. 2(c) demonstrates the mutual-switching between **A**, **B**, and **C** states, where a pulse of 6.0 V for the **A** state, -6.0 V pulse for the **B** state, and a $-6\text{ V} + 2.4\text{ V}$ pulse series for the

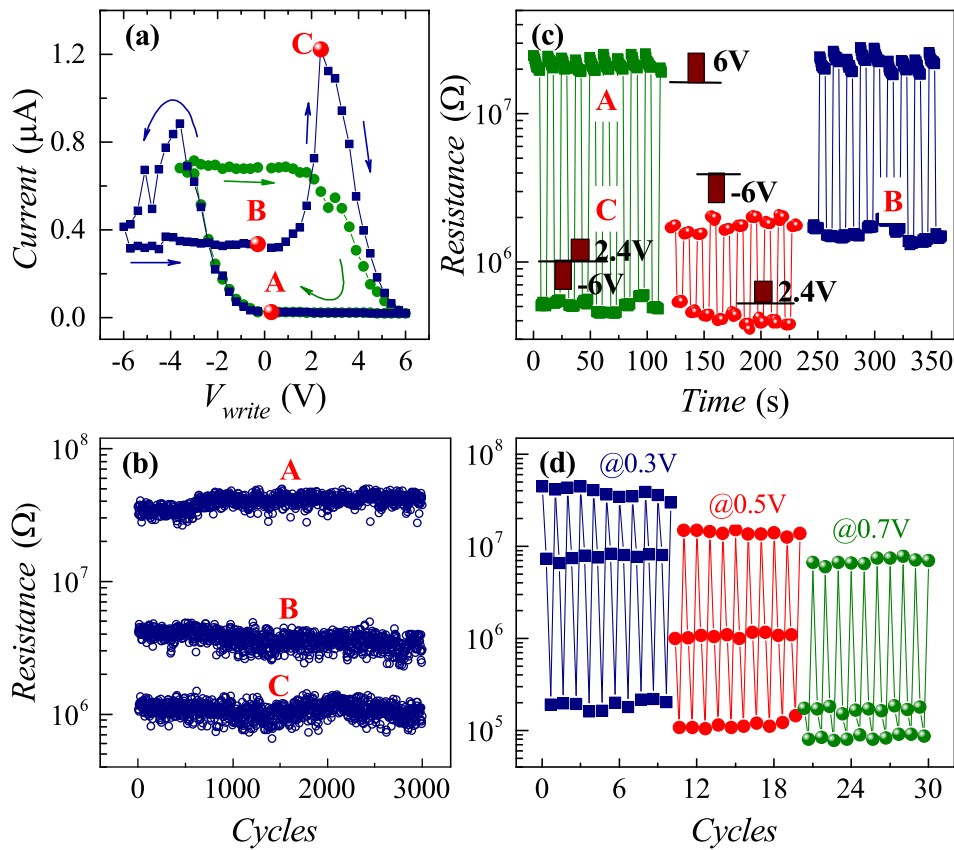


FIG. 2. (a) Current- V_{write} hysteresis loops, measured by 0.1 V after each V_{write} pulse, with $V_{write} \in [-6.0\text{ V}, 6.0\text{ V}]$ and $[-3.6\text{ V}, 6.0\text{ V}]$, respectively. (b) Endurance characters of the A, B, and C states, measured by 0.1 V during the intervals of pulses of 6 V, -6 V, 2.4 V, respectively. (c) Mutual resistance switching between A, B, and C states, measured by 0.5 V after the operation pulses. (d) The resistive switching between A, B, and C states, with the reading voltage of 0.3 V, 0.5 V, and 0.7 V, respectively.

C state. In addition, the A, B, and C states also demonstrate good retention longer than 10^4 s (shown in Fig. S1 in the [supplementary material](#)).

The resistance state and multi-switching behavior also depend on read-voltage. Fig. 2(e) shows the endurance of the A, B, and C states under several read-voltages of 0.3 V, 0.5 V, and 0.7 V, respectively. With the increasing read-voltage, the resistances of all the states are slightly reduced, and the resistance ratio between states A and B is enhanced while that between states B and C is reduced. As shown in Fig. 3, for another sample, the read-voltage dependence of the multi-switching behavior is characterized by the R - V_{write} curves for a series of read-voltages from -1.0 V to 2.1 V. First, the R - V_{write} hysteresis evolves from the butterfly loop at low read-voltage to single-loop (parallelogram-like) at high read-voltage. The disappearance of the butterfly pattern occurs roughly at the read-voltage comparable with the critical voltage. Second, the resistance platform height shows downward-shift with increasing read-voltage. Third, multi-control of the resistance state can be realized easily. For example, given a read-voltage of 2.1 V, a pulse of 6.0 V produces a HR state while a pulse of -6.0 V produces a LR state. On the contrary, if the read-voltage is -2.1 V, a LR state is reached by a pulse of 6.0 V and a HR state by a pulse of -6.0 V. Therefore, for a fabricated CRS device, the read voltage can provide another useful parameter to adjust suitable device's resistance and off/on ratio, being convenient for the real application.

Earlier investigations revealed that the ferroelectric polarization reversal can modulate the barrier of electrode/ferroelectric junctions and is one of the major reasons for the resistance switching in FTJs.¹⁷ To examine this switching

mechanism in our CRS devices, we measured the local piezoresponse hysteresis loops on a bare surface of BTO film. Fig. 4(a) displays the piezoresponse phase- V_{write} hysteresis and the butterfly-like amplitude- V_{write} hysteresis. The phase difference between the two polarization states is $\sim 180^\circ$, and the switching voltage is coincided with the minima of the amplitude- V_{write} loop, identifying the good ferroelectricity for the BTO film.

Considering that the high/low resistance ratio of the CRS device is more than 100 and the two anti-serially connected FTJs in the CRS device are always at LR and HR states, respectively, more than 99% drop of V_{write} will be actually on one FTJ junction with HR state. Fig. 4(b) shows that the voltages at the minima of the amplitude- V_{write} loop

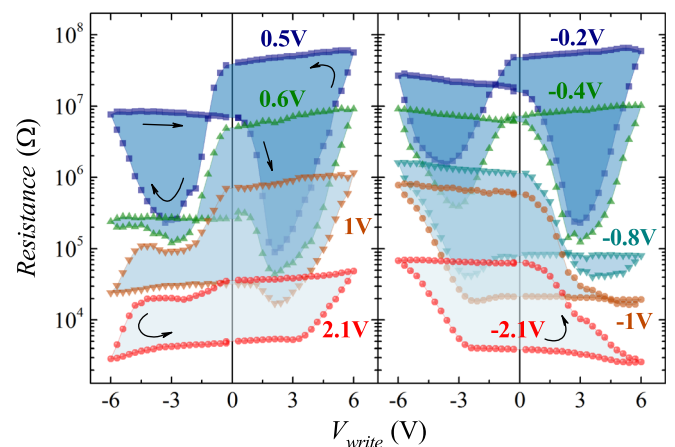


FIG. 3. R - V_{write} hysteresis loops measured under the reading voltages of -2.1 V, -1 V, -0.8 V, -0.4 V, -0.2 V, 0.5 V, 0.6 V, 1.0 V, and 2.1 V, respectively.

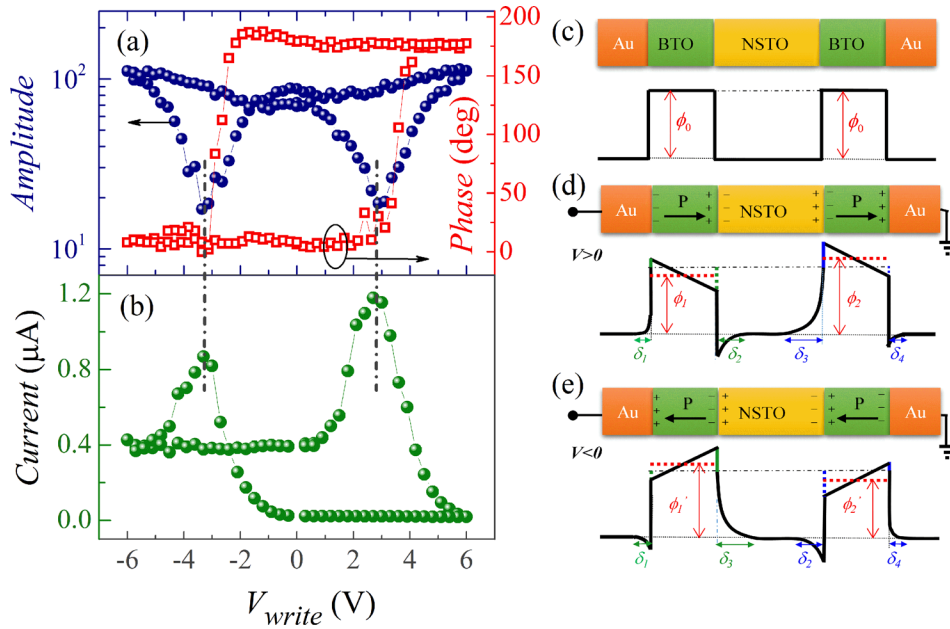


FIG. 4. (a) Hysteretic behavior of the PFM amplitude and phase signals measured on the bare surface of the BTO film as a function of the bias applied via a conducting tip. (b) Current- V_{write} hysteresis behavior measured by 0.1 V after each V_{write} pulse ($-6\text{ V} < V_{write} < 6\text{ V}$). (c), (d), and (e) Schematic diagram of the electronic potential profile of Au/BTO/NSTO/BTO/Au stack, before and after positive and negative pulse voltage stressing, respectively.

and current- V_{write} loop are coincided with each other. This indicates that the minima in the current- V_{write} loop appear near the ferroelectric coercive field, suggesting that the butterfly-like resistance switching is intrinsically correlated with the polarization switching. It is noted that the coercive voltages in the piezoresponse force microscopy (PFM) hysteresis loop is larger than the coercive field of the conventional BTO thin film, which may be induced by the high contact resistance between the PFM tip and the BTO film during the PFM measurement.

The comparison of R - V_{write} behaviors of single-FTJ and CRS devices indicates that the electro-transport of the present CRS device can be described as two anti-serial connected Au/BTO/NSTO junctions. The R - V_{write} behaviors of the single-FTJ are shown in Fig. S2 in the [supplementary material](#). For simplified discussion, the electrostatic potential profile across the Au/BTO/NSTO/BTO/Au structure is drawn in Fig. 4(c), where the initial potential barrier is supposed to be rectangular with a barrier height ϕ_0 .¹⁷ As a V_{write} pulse is applied to the junctions, the remanent polarization of the BTO film gives rise to the bound charges in both ends of the BTO film. The incomplete screening of the bound charges causes additional electrostatic potentials near the Au/BTO and BTO/NSTO interfaces, leading to the variation of the junction barrier profile, as schematically shown in Figs. 4(d) and 4(e) for positive and negative write pulses, respectively. Since the polarization points toward the Au/BTO (or NSTO/BTO) interface, the junction barrier height is lowered and the barrier width is reduced, with a barrier width of δ_4 (or δ_2) at the Au (or NSTO) side, respectively. As the polarization points away from the Au/BTO (or NSTO/BTO) interface on the contrary, however, the junction barrier height is raised and the barrier width is enlarged, with a barrier width of δ_1 (or δ_3) at Au (or NSTO) side, respectively.

Due to the strong influence of interface microstructure and the difference in the density of states at the Fermi level between the Au and n -type NSTO, one has the screen lengths $\delta_2 \neq \delta_3$, $\delta_1 \neq \delta_4$, and both δ_2 and δ_3 are usually greatly larger than δ_1 and δ_4 , respectively.^{17,20,21} Given a rightward polarization (Fig. 4(d)), the average barrier height of the left FTJ is

reduced to ϕ_1 but that of the right FTJ is enhanced to ϕ_2 , satisfying $\phi_1 < \phi_0 < \phi_2$. On the other hand, for a leftward polarization (Fig. 4(e)), the average barrier height of the left FTJ is enhanced to ϕ'_1 while that of the right FTJ is reduced to ϕ'_2 , meeting $\phi'_2 < \phi_0 < \phi'_1$. Consequently, relations $\phi_0 < \phi_2$ and $\phi_0 < \phi'_1$ are satisfied. This means that the average barrier height of the CRS is raised due to the presence of the leftward- or rightward-oriented remanent polarization. This explains why the initial states are certainly in the LR state, since the well-aligned polarization state is not yet established. Once the write-pulse is higher than the critical voltage, enabling the polarization alignment in the BTO layer, the LR-HR state transitions occur.

The butterfly-like R - V_{write} hysteresis is well understood within this framework. Starting from a state with leftward polarization, a positive V_{write} -sweep from 0 to 6.0 V drives the polarization reversal from leftward to rightward, across the resistance valley near the coercive field. The backward sweep of V_{write} from 6.0 V to 0 does not change the rightward polarization so that a HR platform is observed. For the negative sweep from 0 to -6.0 V and then from -6.0 V to 0, a similar sequence occurs and the only difference is that the polarization experiences a rightward-leftward reversal. It is reasonable that the barrier ϕ_2 is not exactly equal to ϕ'_1 , considering the inevitable defects and/or the microstructural inhomogeneity in Au/BTO and NSTO/BTO interfaces. Therefore, the heights of the two HR platforms cannot be identical, leading to the butterfly-like R - V_{write} hysteresis.

A read-voltage gives additional electro-potential to the BTO/Au and BTO/BSTO interfaces, which explains the read-voltage control of the R - V_{write} behavior. On the one hand, the increased read-voltage raises the energy of carriers helping them to flow through the FTJ barriers and therefore downshifts the R - V_{write} hysteresis as a general tendency. On the other hand, the read-voltage is also able to tune the polarization states during the reading processes. Referring to the potential profile in Fig. 4(e), a negative read-voltage will raise the barrier of the left FTJ while reducing the barrier of the right FTJ, while a positive read-voltage does the

opposite. Therefore, the resistance platform in the positive V_{write} region should be higher than, equal to, or lower than that in the negative V_{write} region, if the read-voltage is sufficiently positive, very small, or sufficiently negative, respectively.

As the read-voltage is close to or larger than the coercive field, the polarization state may be destroyed during the reading process, causing the switches between a fully polarized state and a non-polarized state. Consequently, a parallelogram-like R - V_{write} hysteresis is shown in Fig. 3, with read-voltages of 2.1 V and -2.1 V respectively. Considering a possibly weak asymmetry of the junction barrier,²⁰ i.e., $\phi_2 \neq \phi_1'$, the read-voltage needed for two identical resistance platforms will be shifted to a non-zero value to compensate the barrier difference ($\phi_2 - \phi_1'$), which is ~ -0.4 V for the sample shown in Fig. 3.

It should be mentioned that carrier trapping/de-trapping near the ferroelectric/electrode interfaces can also cause the similar resistance switching behavior.^{20,22} However, the temperature- and pulse-time dependent R - V_{write} loop behaviors (shown in Fig. S3 in the [supplementary material](#)) indicate that the ferroelectric switching is the dominant mechanism although the carrier trapping/detrapping may play a minor role in the resistance switching at room temperature. The detail discussion is shown in the [supplementary material](#).

As an intrinsic property of ferroelectricity in the BTO film, the remanent polarization is highly stable, which ensures the good stability of the resistance state of the CRS device. Besides, the fixed coercive field unifies the critical pulse voltage of CRS device, and the inherent fatigue resistance properties of ferroelectric switching in BTO provides a strong backup for the good endurance of resistance switching in the CRS device.²³ Comparing with the VCM-based CRS device, the uniform ferroelectric switching in the FTJ-based CRS device avoids the randomness of filament connection/corruption in the local region and therefore greatly raises the performance of the device. Furthermore, the self-forming ability in the FTJ-based CRS device overcomes the uniform forming problem encountered in many VCM-based CRS devices.

In summary, we have investigated the resistance switching behaviors of a CRS device based on two anti-serial Au/BTO/NSTO ferroelectric tunnel junctions (FTJs). This FTJ-based CRS device shows a stable butterfly-like resistance-voltage hysteresis. It owns the functionality of self-electroforming, multi-switching, and complementary switching, and the resistance ratio can be well tuned by reading voltage besides the operation pulse. These make the FTJ structure great potentials for high performance CRS memristors. Our data demonstrate that the high performance and multi-functionalities of this device are attributed to the stable ferroelectric switching in BTO film where the remanent polarization modulates the junction barriers in the device. The measurement of retention (much longer than 10^4 s) and endurance (much larger than 10^4 times) at high temperature or room temperature is deserved to

be carried out to guarantee performance suitable for real devices in the future.

See [supplementary material](#) for the complete discussion on the switching mechanism of CRS device.

This work was supported by the National Key Research Programme of China (Grant Nos. 2016YFA0300101, 2016YFA0201004), the National Natural Science Foundation of China (Grant Nos. 51301084, 51431006, 11374112), and the Natural Science Foundation of Jiangsu, China (Grant No. BK20130576). This research is also supported by the Hong Kong NSFC/RGC grant (No. N-PolyU517/14) and Strategic Importance Project of The Hong Kong Polytechnic University (No. 1-ZE25).

- ¹A. Siemon, T. Breuer, N. Aslam, S. Ferch, W. Kim, J. van den Hurk, V. Rana, S. Hoffmann-Eifert, R. Waser, S. Menzel, and E. Linn, *Adv. Funct. Mater.* **25**, 6414 (2015).
- ²J. Y. Seok, S. J. Song, J. H. Yoon, K. J. Yoon, T. H. Park, D. E. Kwon, H. Lim, G. H. Kim, D. S. Jeong, and C. S. Hwang, *Adv. Funct. Mater.* **24**, 5316 (2014).
- ³V. Y. Aristov, O. V. Molodtsova, C. Laubschat, V. M. Zhilin, I. M. Aristova, V. V. Kveder, and M. Knupfer, *Appl. Phys. Lett.* **97**, 113103 (2010).
- ⁴L. Wun-Cheng, L. Kuan-Liang, H. Jiun-Jia, L. Chung-Lun, and H. Tuo-Hung, *IEEE Electron Device Lett.* **33**, 597 (2012).
- ⁵S. J. Lee, K. S. Oh, Y. G. Ahn, K. Cho, and K. Eshraghian, in *2013 IEEE Eighth International Conference on Intelligent Sensors, Sensor Networks and Information Processing* (2013), p. 485.
- ⁶E. Linn, R. Rosezin, C. Kugeler, and R. Waser, *Nat. Mater.* **9**, 403 (2010).
- ⁷Z. Yan, Y. Guo, G. Zhang, and J. M. Liu, *Adv. Mater.* **23**, 1351 (2011).
- ⁸C. Baeumer, C. Schmitz, A. H. Ramadan, H. Du, K. Skaja, V. Feyer, P. Muller, B. Arndt, C. L. Jia, J. Mayer, R. A. De Souza, C. Michael Schneider, R. Waser, and R. Dittmann, *Nat. Commun.* **6**, 8610 (2015).
- ⁹M.-J. Lee, C. B. Lee, D. Lee, S. R. Lee, M. Chang, J. H. Hur, Y.-B. Kim, C.-J. Kim, D. H. Seo, S. Seo, U. I. Chung, I.-K. Yoo, and K. Kim, *Nat. Mater.* **10**, 625 (2011).
- ¹⁰W. Lee, J. Park, S. Kim, J. Woo, J. Shin, G. Choi, S. Park, D. Lee, E. Cha, B. H. Lee, and H. Hwang, *ACS Nano* **6**, 8166 (2012).
- ¹¹Z. B. Yan and J. M. Liu, *Ann. Phys.* **358**, 206 (2015).
- ¹²D. S. Jeong, R. Thomas, R. S. Katiyar, J. F. Scott, H. Kohlstedt, A. Petraru, and C. S. Hwang, *Rep. Prog. Phys.* **75**, 076502 (2012).
- ¹³K. D'Aquila, C. Phatak, M. V. Holt, B. D. Stripe, S. Tong, W. I. Park, S. Hong, and A. K. Petford-Long, *Appl. Phys. Lett.* **104**, 242902 (2014).
- ¹⁴S. Yu, J. Liang, Y. Wu, and H. S. Wong, *Nanotechnology* **21**, 465202 (2010).
- ¹⁵S. Dong, J.-M. Liu, S.-W. Cheong, and Z. Ren, *Adv. Phys.* **64**, 519 (2015).
- ¹⁶G. Radaelli, D. Gutierrez, F. Sanchez, R. Bertacco, M. Stengel, and J. Fontcuberta, *Adv. Mater.* **27**, 2602 (2015).
- ¹⁷V. Garcia and M. Bibes, *Nat. Commun.* **5**, 4289 (2014).
- ¹⁸Y. W. Yin, J. D. Burton, Y. M. Kim, A. Y. Borisevich, S. J. Pennycook, S. M. Yang, T. W. Noh, A. Gruverman, X. G. Li, E. Y. Tsymlal, and Q. Li, *Nat. Mater.* **12**, 397 (2013).
- ¹⁹A. Chanthbouala, V. Garcia, R. O. Cherifi, K. Bouzehouane, S. Fusil, X. Moya, S. Xavier, H. Yamada, C. Deranlot, N. D. Mathur, M. Bibes, A. Barthelemy, and J. Grollier, *Nat. Mater.* **11**, 860 (2012).
- ²⁰R. Soni, A. Petraru, P. Meuffels, O. Vavra, M. Ziegler, S. K. Kim, D. S. Jeong, N. A. Pertsev, and H. Kohlstedt, *Nat. Commun.* **5**, 5414 (2014).
- ²¹L. Pintilie and M. Alexe, *J. Appl. Phys.* **98**, 124103 (2005).
- ²²Y. B. Lin, Z. B. Yan, X. B. Lu, Z. X. Lu, M. Zeng, Y. Chen, X. S. Gao, J. G. Wan, J. Y. Dai, and J. M. Liu, *Appl. Phys. Lett.* **104**, 143503 (2014).
- ²³F. Liu, Y. Zhou, Y. Wang, X. Liu, J. Wang, and H. Guo, *npj Quant. Mater.* **1**, 16004 (2016).